Text-Guided Texturing by Synchronized Multi-View Diffusion

Yuxin Liu Minshan Xie Hanyuan Liu Tien-Tsin Wong The Chinese University of Hong Kong

{yxliu22, msxie, liuhy, ttwong}@cse.cuhk.edu.hk

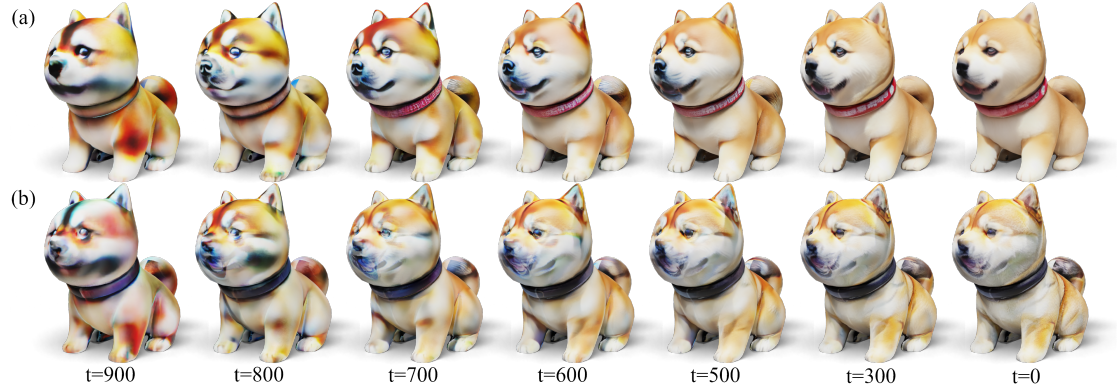


Figure 1. Visualization of RGB textures at different intermediate denoising steps. (a) With the proposed MVD, consensus on surface color layouts are reached from the early stage of the diffusion process. (b) Without MVD and lack of consensus, obvious seams, ghosting, fragmentation artifacts are observed at the end as views are inconsistent to each other.

Abstract

This paper introduces a novel approach to synthesize texture to dress up a given 3D object, given a text prompt. Based on the pretrained text-to-image (T2I) diffusion model, existing methods usually employ a project-and-inpaint approach, in which a view of the given object is first generated and warped to another view for inpainting. But it tends to generate inconsistent texture due to the asynchronous diffusion of multiple views. We believe such asynchronous diffusion and insufficient information sharing among views are the root causes of the inconsistent artifact. In this paper, we propose a synchronized multi-view diffusion approach that allows the diffusion processes from different views to reach a consensus of the generated content early in the process, and hence ensures the texture consistency. To synchronize the diffusion, we share the denoised content among different views in each denoising step, specifically blending the latent content in the texture domain from views with overlap. Our method demonstrates superior performance in generating consistent, seamless, highly detailed textures, comparing to state-of-the-art methods.

1. Introduction

Existing rendering systems predominantly utilize polygonal geometric primitives, like triangles, and apply texture mapping to enhance visual appeal. These textures are sourced from photographs, manual paintings, or procedural computations [6]. However, most of these texture acquisition methods require domain specific expertise and manual efforts, which is of course, not as convenient as generating textures from a text prompt. In this paper, we introduce a method for generating textures for a 3D object based on text descriptions.

There exists a few works [4, 30] trying to achieve the above goal. Typically, they generate a view using depth-conditioned text-to-image (T2I) models, project this view onto the object's surface, and render the partially textured object from a rotated camera position. Next, the missing texture regions are filled using inpainting from the current viewpoint with the T2I model. These project-and-inpaint methods often result in texture inconsistencies, as shown in Fig. 5. Each view, diffused separately, lacks adequate consistency constraints, failing to ensure a seamless appearance from various viewpoints.

The primary issue, we believe, lies on the *asynchronous* diffusion among views. Note that even with depth map as guidance, it cannot fully align content nor avoid the error accumulation in sequential inpainting due to the limited

context from previous textures. Our solution is a *synchronized multi-view diffusion* approach. This method achieves early-stage content *consensus*, essential for consistent structure and error correction across views.

In order to synchronize the diffusion among different views, it is necessary to allow the denoised content being shared among different views in each denoising step. The overlapped region among different views on the textured object (Fig. 2, left) serves as the information exchange sites. During each denoising step, we share (blend in our case) the latent from different views in the UV texture domain, if they have an overlap. The texture consensus can be obtained during the early stage of denoising as demonstrated in Fig 1a. Note that, all views share the same importance during this consensus process, i.e. no view is overriding the others during the denoising.

With the proposed approach, we obtain plausible and highly detailed textures for arbitrarily given 3D objects. Please refer to the numerous results presented in this paper and the supplement. We have evaluated the results generated by our synchronous multi-view diffusion, via quantitative and qualitative evaluations. Superior performance is achieved comparing to state-of-the-art methods. In summary, our contributions can be summarized as follow.

- We identify the problem of existing methods stemmed from the asynchronous diffusion, and propose a novel synchronous multiview diffusion approach to generate text-guided texture on target 3D objects.
- We proposed a practical solution to generate consistent, seamless, plausible, highly detailed textures given a text prompt.
- We conduct extensive experiments on a variety of 3D meshes, which shows superior editing performance compared with state-of-the-art methods.

2. Related Work

Texture Synthesis Methods Early works on texture related topic mainly focused on generating 2D and 3D tileable texture maps from exemplars [1, 7, 15, 16], and applying them to a given object in a seamless way [5, 28]. Existing works also explored the correlation between surface structures and texture details, enabling geometry-aware synthesis and transfer of texture details [20, 21, 38]. However, both rule-based methods and early machine learning models are of limited capacity, synthesizing textures with rich semantics on complicated geometry is not feasible at that time.

In the recent few years, deep learning methods, especially convolutional neural networks exhibit their strong capabilities on image-related tasks. Texture synthesis methods in the recent years are based on popular generative models such as GANs [8, 12], VAEs [14, 37] and state-of-the-art diffusion model [10, 35], to sample from a prior trained on

voxels [34, 42], point clouds [26, 39, 40] and implicit representations [9, 17, 19, 25] of a textured 3D object. However, generating highly-detailed texture for a given mesh is seldom discussed, even it is demanded.

Zero-shot Texturing Using Text-Image Prior Recently, priors trained on large scale text-image data empowered researches on various image generation and modification task. Due to the lack of large-scale 3D dataset with high quality annotation for training a prior natively in 3D, many previous 3D content generation works alternatively choose to use 2D priors, and achieved strong zero-shot ability when paired with carefully designed sampling pipelines. Following this idea, several works in texture generation [13, 32, 33] distill gradients from CLIP model [29], which trained with correlate text and image using contrastive learning. These gradients are used to update rendered views of a 3D object iteratively, to make it conforms to the given text.

Score distillation methods [11, 18, 23, 27] on the other hand, distill gradients from state-of-the-art image generation models, diffusion models [10, 35]. For texture generation, SDS-based methods add noise to a rendered view of the current 3D object, and use the diffusion model to reconstruct the noiseless input. By this means, the result clean view is incorporated with prior knowledge from the diffusion model, and can be used to update the object texture. However, diversity and quality of their output, as well as the optimization time are unsatisfactory compared to normal diffusion inference on a 2D image.

TEXTure [30] and Text2Tex [4] on the other hand, approached this problem by progressive inpainting with a depth-conditioned diffusion model [31]. Their methods start by generating a view of the object using the diffusion model with the depth map rendered from the mesh as control, and then projecting the screen-space textures onto the object surface. In every iteration, they rotate the object by an angle, and inpaint the partially visible texture from this new view. These methods achieve better texture sharpness and faster running time, but may suffer from obvious seams and over-fragmentation, due to the asynchronous nature of their diffusion processes. A recent work [3] attempts to address the inconsistency problem by performing a complete round of project-and-inpaint in each denoising time-step, in an auto-regressive manner. In contrast, our method treats each view equally, latent information from all views are fused in a synchronized fashion, in order to reach a consensus in terms of content structure and color distribution. We show that consensus can be quickly reached in the very early stage of denoising process (Fig. 1a).

3. Diffusion Model Preliminaries

Denoising Diffusion Models are generative neural networks trained to reverse a Markov process which diffuses its input data to pure Gaussian noise. During training, given input

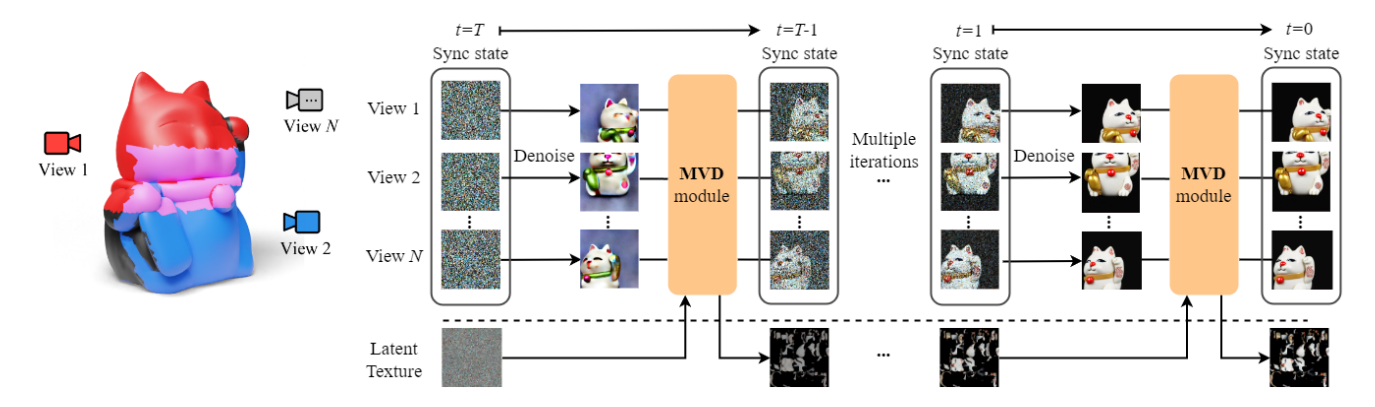


Figure 2. Left: An illustration of information exchange in overlapped region (pink region) at intermediate steps of diffusion. Without information exchange, denoising result in different views of the same object could diverge into different directions, leading to seams when projecting to an output texture. Right: To tackle this issue, we propose a Multi-View Diffusion module that fuses intermediate steps of the denoising process, basing the next denoising step on a consensus of the current step. Here, we illustrate how MVD synchronizes and fuses view information from timesteps T to 0.

data x, a fixed forward process gradually destroys the information in each intermediate time step t and eventually approaches to a pure Gaussian noise x_T at t=T. Then a neural noise predictor $\epsilon_{\theta}(x_t,t)$ (e.g., a U-Net) is trained to estimate the true noise ϵ mixed into the input, given arbitrary time step t and corresponding noisy data x_t . Inference can be performed by sampling from the Gaussian noise at time T, and iteratively removing part of the predicted noise to reach a fully denoised x_0 .

In our work, we utilize Stable Diffusion model [31], which is trained to denoise in low-resolution latent space $z = \mathcal{E}(x)$ encoded by a pre-trained VAE encoder \mathcal{E} , as it can significantly reduce the computational cost. Then, an image can be generated through the following steps:

- 1. Sample a noise image z_T from the standard normal distribution.
- 2. For each intermediate diffusion time step t:
 - (a) Given noisy latent image z_t , the model predicts the noise $\epsilon_{\theta}(z_t,t)$ in the current latent image. We can obtain a clean intermediate state $z_{0|t}$ by removing the noise from z_t (modifications on $z_{0|t}$ can be applied to affect the subsequent denoising process).
 - (b) Compute latent image z_{t-1} at the next time step t-1, which is a linear combination of z_t and $z_{0|t}$ using time-step-related coefficients.
- 3. Decode the fully denoised z_0 with the VAE decoder \mathcal{D} to obtain the output image $x = \mathcal{D}(z_0)$.

In addition to text conditioning using built-in attention mechanisms, several external encoders and adapters [24, 41] have been designed to enable diffusion models to condition on other modalities. ControlNet as one of these methods, allows diffusion models to generate images conditioned on screen-space depth or normal maps.

4. Synchronized Multi-View Diffusion

With the given object geometry and a known camera, the ground truth depth map or normal map can be rendered to condition the above 2D image generation, making it possible to generate 2D views of the desired textured 3D object. Therefore, we design an object texturing framework as follow, in order to perform zero-shot texture generation using a pretrained T2I diffusion model without texture domain knowledge. We first surround the target 3D object m with multiple cameras $\{v_1, v_2, \cdots v_n\}$, each covers part of the object. Then a T2I diffusion process is assigned to synthesize each of these 2D views $\{z_t^{(v_1)}, z_t^{(v_2)}, \cdots, z_t^{(v_n)}\}$, with text prompt y as guidance and conditional images (depth or normal map rendered from the corresponding viewpoints) as the condition. With sufficient views, we can obtain the complete texture map covering the whole object, by projecting the generated pixels from each view onto the object surface, which in turn can be mapped to the texture domain (UV space), as illustrated in Fig. 2.

The key challenge here is on how to generate views that are inconsistent to each other. Texture map with severe fragmentation and seams may be generated when directly combining each view generated through a separate diffusion process (Fig. 1b). One can use postprocessing smoothing to reduce the obvious seams, but with the trade-off of overblurriness. Our major contribution lies on how to ensure the consistency among the generated views, and hence prevent obvious fragmentation and seams, so that sharp and highly detailed textures can be obtained.

The root cause of the inconsistency among generated views, is that the corresponding diffusion processes of views are performed in a more-or-less independent fashion. Note that the rendered conditional images are insufficient to ensure the consistency of textured views in medium or

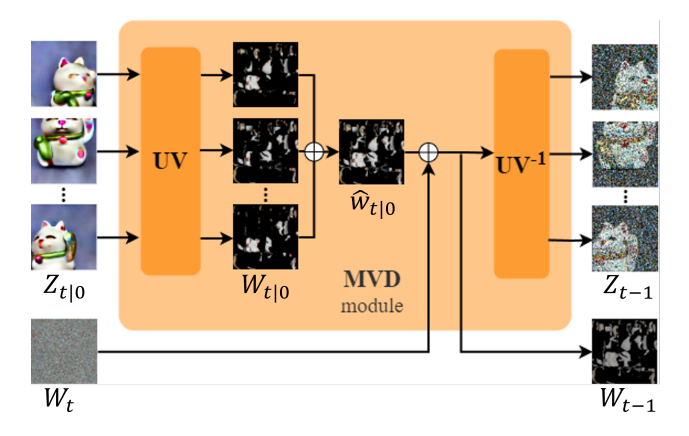


Figure 3. A zoom-in diagram of MVD module. Here, denoised views are first projected to partial textures in the UV texture domain and aggregated into a complete clean latent texture. Then we can sample the latent texture of the next time step based on this clean texture, and project to screen space to get consistent views.

fine scales. In order to foster a consistent texture at different scales, we need to share the latent information among views since the beginning of the denoising process (from time step T). To do so, the latent values of views are shared among each other between every denoising step. We called this synchronized multi-view diffusion (MVD). Fig. 2(right) illustrates how information among views are shared and synchronized with MVD from the denoising time-steps T to 0. This sharing can be done via the overlapping among views (Fig. 2(left)) in the texture domain. The latent values from different views on the overlapping area can be blended with appropriate weights, and combined values are then used for next round of denoising.

Such latent value sharing allows the diffusion processes of all views to reach a consensus of the generated texture in terms of overall structure and color distribution in the early stage of the denoising process. Fig. 1a visualizes how fast the consensus is reached in generating the texture, in comparing to the one without information sharing in Fig. 1b.

4.1. Multi-View Diffusion in Texture Domain

Our Multi-View Diffusion module utilizes the overlapping region in UV texture space for synchronization. Instead of pairwise screen-space warping, we choose to use the UV mapping as a pre-established connection among all views. This mapping allows us to align predictions from multiple views to this canonical texture layout, and distribute the synchronized results to each individual views through rendering. The detailed procedures are as follows.

At initial time step T, we first initialize a latent texture W_T with standard normal distribution. Then we render the source mesh from views $V = \{v_i\}_{i=1}^N$ using this map as the texture, to obtain 3D-consistent initial views $Z_T = \{z_T^{(v_i)}\}_{i=1}^N$ of the object. Background pixels are ran-



Figure 4. An illustration of how the forwardly projected pixels are disjoint in UV space, and how filling and masking are applied to obtain a partial textures with large patches of valid texels.

domly sample with the same noise distribution, and then composited with the rendered foreground object using the object mask.

At each time step t, we can compute the 3D-consistent Z_{t-1} of the next time step based on noiseless view $Z_{0|t} = \{z_{0|t}^{(v_i)}\}_{i=1}^N$ estimated by the model. But this computation is done separately for each view. To guarantee the consistency among views, we need to project $Z_{0|t}$ to UV texture space for computation, like in the initialization step. Projecting $Z_{0|t}$ to UV space yields the partially covered textures $W_{0|t} = \mathbf{UV}(Z_{0|t})$. Here \mathbf{UV} denotes the mapping from screen space to texture space, and \mathbf{UV}^{-1} denotes mapping from texture space back to screen space. The current-step clean texture can be obtained through averaging these partial textures at each overlapping texel:

$$\hat{W}_{0|t} = \frac{\sum_{i=1}^{N} w_{0|t}^{(v_i)}}{\sum_{i=1}^{N} M(v_i) + \gamma}$$
(1)

 $w_{0|t}^{(v_i)}$ denotes the partial texture projected from view v_i , $M(v_i)$ denotes a triangle visibility mask which marks the regions in $w_{0|t}^{(v_i)}$ visible in view v_i , such that only visible texels are taken into account for averaging; and γ is a small constant to avoid division-by-zero in the masked-out regions.

Based on the diffusion sampling method introduced in Sec. 3, the texture in next time step W_{t-1} can be sampled using $\hat{W}_{0|t}$ and W_t (additional noise should be added in UV space as the variance term in diffusion sampling). Finally, this texture is mapped back to corresponding views $Z_{t-1} = \mathbf{U}\mathbf{V}^{-1}(W_{t-1})$. Fig. 3 illustrates this MVD process. These generated views should have consistent textures on corresponding regions. To assign background with valid latent noise, we encode a random solid color image and add proper noise based the current time step.

Our method implements the screen-to-texture projection UV using back-propagation supported by a differentiable renderer. This implementation has a drawback that only texels visible on screen can receive non-zero gradients, such that texels with valid latent values appear as disconnected dots instead of complete patches on the partial latent textures, as pixels are forwardly projected onto UV space. Information exchange will be compromised if multiple such textures are aggregated, due to the sparsity. To tackle this

issue, we simply apply a Voronoi-based filling [2] to propagate the latent texels to fill up all empty regions in the UV space. Fig 4 shows the latent texture which filled with Voronoi diagram. The fully-filled latent texture are then masked according to a triangle visibility mask $M(v_i)$, such that the propagation will not exceed the boundary of regions visible to view v_i , as shown in Fig 4. These filled textures are now ready for aggregation since they are free of the sparsity problem mentioned above.

4.2. Self-attention Reuse

Due to the fact that multiple views of the same object tend to develop similar looks when they are concatenated into a single image during denoising [36], we modify the behavior of batched self-attention computation in the pre-trained denoising U-Net to enable attention to other views in the same batch. Benefiting from the pre-trained self-attention layers, spatially distant views can now develop highly-related appearances even overlap in UV-space is small or unavailable. Nevertheless, we observed certain degradation of generated details when pairwise view attentions are used. Based on the observation, we propose two attention schemes to achieve the appearance harmonization in different stages of denoising.

$$\operatorname{Attention}(v_i) = \begin{cases} \beta \cdot \operatorname{SA}(v_i, v_{\{i-1, i, i+1\}}) & \text{for } t > t_{\operatorname{ref}} \\ + (1-\beta) \cdot \operatorname{SA}(v_i, v_{\operatorname{ref}}) & \\ \operatorname{SA}(v_i, v_{\{i-1, i, i+1\}}) & \text{otherwise} \end{cases}$$
 where
$$\operatorname{SA}(v_m, v_n) \text{ denotes that we use the pre-trained self-}$$

where $\mathrm{SA}(v_m,v_n)$ denotes that we use the pre-trained self-attention layer to attend to view v_n when calculating the attention results of view v_m in the denoising U-Net. We use t_{ref} to denote the time step where we switch between two attention schemes. To enforce a global harmonization in the early stage of denoising, we apply two attention components before time step t_{ref} : (1) attention to the view itself, its left, and its right neighbors; and (2) attention to a reference view v_{ref} , which can be the default front view or a manually selected view. These two components are balanced by a weight factor β . In the remaining denoising steps, we disable the reference view attention to avoid content invisible from the reference view v_{ref} , from being impaired by enforcing attention to the reference view.

4.3. Finalizing the Texture

Despite that we can denoise a latent texture to a noiseless state to obtain the final texture, we choose not to do so, due to the following two reasons. Firstly, a latent texture generated through projecting screen-space latent to a texture is not viable for directly decoding to the final RGB texture, as stretching and rotation in the latent texture are likely to cause mismatching with the trained distribution of the decoder. Secondly, we observed that sharpness of the generated results could drop during the last few denoising steps

(in which high-frequency details are forming) when Multi-View Diffusion is enforced.

Therefore, we choose to conduct the final phase of denoising in screen space, with self-attention reuse enabled. The final RGB texture can then be extracted from fully denoised views $Z_0 = \{z_0^{(v_i)}\}_{i=1}^N$ through decoding, projecting to texture space, and aggregation. Note that although latent texture guarantees the 3D consistency of latents, the high frequency details in the decoded images are not consistent at pixel-level. In order to retain the high-frequency details in the unified result, we propose to perform per-texel weighted combination based on their geometric contribution. Inspired by [4, 30], we utilize the cosine similarities between per-pixel normal vectors and the viewing direction to determine the weight of each contributing pixel, as geometries facing away from the camera are less reliable. Hence, we compute the combined color value as follows.

$$\operatorname{Texture}(Z_0) = \frac{\sum_{i=1}^{N} \mathcal{D}(z_0^{(v_i)}) \odot \mathbf{U} \mathbf{V}(\theta^{(v_i)})^{\alpha}}{\sum_{i=1}^{N} \mathbf{U} \mathbf{V}(\theta^{(v_i)})^{\alpha} + \gamma}$$
(3)

where \odot denotes element-wise (texel-wise) multiplication, α is an exponent to adjust the smoothness of blending and γ is a small constant to avoid division-by-zero in the masked-out regions; $\theta^{(v_i)}$ is the weight map for view v_i and it is calculated as the cosine similarity between the viewing direction v_i and the normal vector, with each element calculated as.

$$\theta^{(v_i)}(p) = \frac{\vec{v}_i(p) \cdot \vec{n}_m(p)}{\|\vec{v}_i(p)\| \|\vec{n}_m(p)\|},\tag{4}$$

where p donates the 3D surface point on object m, corresponding to the screen pixel of interest, $\vec{v}_i(p)$ is the viewing direction from p to view v_i and $\vec{n}_m(p)$ is the normal vector at p. The formulation of cosine similarity intuitively means the view facing directly to the surface point is more important. In all our experiments, we set $\alpha=6$ and disable the Voronoi-based filling during the texture project for sharpness preservation.

5. Results

5.1. Implementation Details

In all our experiments, we have 10 cameras (views) to cover the object. Eight orthographic cameras are placed along the equator surrounding the object with a 45° interval, and two additional cameras at elevated locations pointing towards the top of the object. Each view has a latent resolution of 96×96 to reduce the aliasing. The UV texture has a high latent resolution of $1,536\times1,536$ to prevent color blocks in rendered latent views in case the mesh has low texel-density regions. To encourage the model to generate views with expected orientation, we append directional keyword



Figure 5. Gallery of objects textured by our method. Text prompts from top to bottom: "photo of Batman, sitting on a rock", "teddy bear wearing superman costume", "photo of a beautiful magpie", "A cute shiba inu dog" and "Blue and white pottery style lucky cat with intricate patterns".

(e.g., "front view") to the text prompt of each view automatically, based on its camera position. Our method takes around 60 to 150 seconds to denoise the above mentioned views, depending on the number of denoising steps. We developed our diffusion pipeline based on Stable Diffusion v1-5 and ControlNet module v1-1 (normal and depth) of Huggingface Diffusers library, and our projection functions are implemented using Pytorch3D.

5.2. Comparison with State-of-the-Art Methods

In this section, we compare our results with four state-ofthe-art methods, including TEXTure [30], Text2Tex [4], Meshy [22], and TexFusion [3]. For the former three methods with public released code or service, we textured a given mesh with the same prompt, and rendered the mesh with texture produced by each method. Fig. 5 visually compares our results with these three methods. TexFusion, on the other hand, have not released their code by the time this paper is prepared, thus we run our method with the same text prompt on a similar objects and render with a similar configuration (Fig. 6). More results of our method are shown in Fig. 7 to illustrate the effectiveness and generalizability of our method.

Comparison with TEXTure and Text2Tex. TEXTure [30] and Text2Tex [4] are two progressive inpainting methods that performs texturing by iteratively warping painted tex-



Figure 6. Comparison with TexFusion. Same prompts with similar meshes are used as input to our method. A similar lighting setup is used to render the images. Please refer to Fig. 1 & 6 in [3] for comparison. Results of [3] are not included as we have not yet received the permission to use.

ture to new views for inpainting. Despite that their inpainting reworks part of the existing textured region to reduce seams, their methods are still suffer from over-fragmentation and obvious seams, especially at the back of the object, as shown in Fig. 5. On the other hand, by reusing self attention to attend to other views, our methods significantly improves the visual quality and style consistency of the texture as viewed from different angles.

Comparison with Meshy. A commercial software named Meshy [22] has shown better consistency in many test cases compared to TEXTure and Text2Tex. Their method produces highly contrasted content than ours. However, it also tends to generate over-saturated colors and misinterpretation of prompts, possibly related to aggressive hyperparameters and prompt engineering in the background Fig. 5. Their method also shows significant inconsistency or blank regions probably due to self-occlusion.

Comparison with TexFusion. Although TexFusion [3] adopts a similar latent texture approach, we observed better view consistency and finer details in our results, compared to the limited sample output currently available (Fig. 6). We hypothesize that our method benefited from our real synchronized denoising (i.e., non auto-regressive), reinforced by self attention reuse. However, more in-depth comparison and quantitative evaluation can only be conducted when their code is released.

Quantitative Evaluation.

In view of the availability of source codes, we can only select TEXTure [30], Text2Tex [4] and Meshy [22] for quantitative comparison. Here we compute their Fréchet Inception Distance (FID) in our evaluation. FID measures the difference between the output distribution of original Stable Diffusion with ControlNet, and the rendering of textured objects with textures generated by each method, similar to the metric used in [3]. Ideally, such difference should be as small as possible, because textures are derived from the pretrained T2I model. The quantitative evaluation shows that our method achieves the best FID score compared to other methods.

Table 1. Quantitative evaluation.

Methods	FID score ↓
Meshy	92.1418
Text2Tex	74.9667
TEXTure	78.6683
Ours	61.6550

5.3. Ablation Study

Multi-View Diffusion Module Fig. 8 compares the results with and without our Multi-View Diffusion module. In the experiment without MVD module, we initialize 3D consistent initial latent noise and denoise each view individually using default Stable Diffusion and ControlNet pipeline. The final texture of the case without MVD exhibits severe ghosting artifact, because the generated appearances from different views are significantly different. Without MVD, there is no consensus in content among different views. This proves that MVD module is essential for alignment and localization of surface details on the textured object.

Self-attention Reuse We also examined the effect of self-attention reuse. When MVD is performed without attention reuse, consensus on the object appearance some times could be difficult to reach in the early diffusion process, leaving conflict appearance in the end result. In certain extreme cases, this also leads to redundant or incomplete content on the object surface. For instance, the suit of the Jackie Chan figure is colored differently for its front and back sides. (Fig. 9). Therefore self-attention reuse can compensate the MVD in reaching consensus for certain cases, especially when the overlap among views is insufficient. This is the case of Jackie Chan figure in which the overlap between front and back views is limited.

5.4. Limitations

Despite our method performs well in generating consistent and high-quality textures, we observe the following limitations. Firstly, the pre-trained model has a bias towards generating common views (e.g., front view) of the object specified in the text prompt, making it unlikely to generate proper bottom view of the object (e.g., it may paint a front view of a shoe on the bottom face of a shoe mesh). We believe this limitation is inherited from the pre-trained model, and is hard to fully circumvent using techniques like directional prompt and depth-guided generation adopted in our method. Secondly, our method does not guarantee perfect boundaries at depth discontinuities in the denoised views (e.g., boundaries of self-occluding geometry or between foreground and background), this may lead to problems during RGB texture extraction and cause colors bleeding to unconnected regions. A potential solution is to introduce optimization based extraction method with perceptual losses or mask out the unreliable boundaries before projecting to the



Figure 7. Gallery of objects textured by our method. Corresponding text prompt is underneath each textured object.



Figure 8. Ablation study of Multi-View Diffusion module (MVD).



Figure 9. Ablation study of Self-attention reuse (SAR).

texture.

6. Conclusion

In this paper, we present Synchronized Multi-View Diffusion, which synthesizes consistent and high-quality tex-





Figure 10. Failure cases. The tail of the dog does not have a clear silhouette in the end diffusion result, which cause incorrect projection to other part of the geometry.

tures in a zero-shot setting, by utilizing the pre-trained T2I latent diffusion models. With sharing information among views in each intermediate denoising steps through overlapping regions in texture space, our method solves the over-fragmentation and seam problems of existing progressive inpainting methods. Furthermore, our method utilizes the pretrained self attention layers as an additional assurance for consistency, further eliminating inconsistent results. Both qualitative and quantitative results demonstrate the effectiveness of our method. Our method meets the need of visual consistency and quality for practical use, with comparable or even better inference time compared to that of existing methods. We hope our work can draw interest in exploring different designs in achieving synchronized diffusion, further addressing the limitations of current methods.

References

- [1] Michael Ashikhmin. Synthesizing natural textures. In *Proceedings of the 2001 symposium on Interactive 3D graphics*, pages 217–226, 2001. 2
- [2] Franz Aurenhammer. Voronoi diagrams—a survey of a fundamental geometric data structure. ACM Computing Surveys (CSUR), 23(3):345–405, 1991. 5
- [3] Tianshi Cao, Karsten Kreis, Sanja Fidler, Nicholas Sharp, and KangXue Yin. Texfusion: Synthesizing 3d textures with text-guided image diffusion models. In *Proceedings of* the IEEE/CVF International Conference on Computer Vision (ICCV), 2023. 2, 6, 7
- [4] Dave Zhenyu Chen, Yawar Siddiqui, Hsin-Ying Lee, Sergey Tulyakov, and Matthias Nießner. Text2tex: Text-driven texture synthesis via diffusion models. *arXiv preprint arXiv:2303.11396*, 2023. 1, 2, 5, 6, 7
- [5] David S Ebert. Texturing & modeling: a procedural approach. Morgan Kaufmann, 2003. 2
- [6] David S. Ebert, F. Kenton Musgrave, Darwyn Peachey, Ken Perlin, and Steve Worley. *Texturing and Modeling: A Proce*dural Approach, Third Edition. Morgan Kaufmann Publishers, 2003. 1
- [7] Alexei A Efros and Thomas K Leung. Texture synthesis by non-parametric sampling. In *Proceedings of the seventh IEEE international conference on computer vision*, pages 1033–1038. IEEE, 1999. 2
- [8] Ian Goodfellow, Jean Pouget-Abadie, Mehdi Mirza, Bing Xu, David Warde-Farley, Sherjil Ozair, Aaron Courville, and Yoshua Bengio. Generative adversarial nets. Advances in neural information processing systems, 27, 2014. 2
- [9] Anchit Gupta, Wenhan Xiong, Yixin Nie, Ian Jones, and Barlas Oğuz. 3dgen: Triplane latent diffusion for textured mesh generation. arXiv preprint arXiv:2303.05371, 2023.
- [10] Jonathan Ho, Ajay Jain, and Pieter Abbeel. Denoising diffusion probabilistic models. *Advances in neural information processing systems*, 33:6840–6851, 2020. 2
- [11] Ajay Jain, Ben Mildenhall, Jonathan T Barron, Pieter Abbeel, and Ben Poole. Zero-shot text-guided object generation with dream fields. In *Proceedings of the IEEE/CVF Conference on Computer Vision and Pattern Recognition*, pages 867–876, 2022. 2
- [12] Tero Karras, Samuli Laine, and Timo Aila. A style-based generator architecture for generative adversarial networks. In Proceedings of the IEEE/CVF conference on computer vision and pattern recognition, pages 4401–4410, 2019.
- [13] Nasir Mohammad Khalid, Tianhao Xie, Eugene Belilovsky, and Tiberiu Popa. Clip-mesh: Generating textured meshes from text using pretrained image-text models. SIGGRAPH Asia 2022 Conference Papers, 2022. 2
- [14] Diederik P Kingma and Max Welling. Auto-encoding variational bayes. arXiv preprint arXiv:1312.6114, 2013. 2
- [15] Johannes Kopf, Chi-Wing Fu, Daniel Cohen-Or, Oliver Deussen, Dani Lischinski, and Tien-Tsin Wong. Solid texture synthesis from 2d exemplars. *ACM Trans. Graph.*, 26 (3):2–es, 2007. 2

- [16] Vivek Kwatra, Irfan Essa, Aaron Bobick, and Nipun Kwatra. Texture optimization for example-based synthesis. In ACM SIGGRAPH 2005 Papers, pages 795–802. 2005. 2
- [17] Muheng Li, Yueqi Duan, Jie Zhou, and Jiwen Lu. Diffusionsdf: Text-to-shape via voxelized diffusion. 2023 IEEE/CVF Conference on Computer Vision and Pattern Recognition (CVPR), pages 12642–12651, 2022. 2
- [18] Chen-Hsuan Lin, Jun Gao, Luming Tang, Towaki Takikawa, Xiaohui Zeng, Xun Huang, Karsten Kreis, Sanja Fidler, Ming-Yu Liu, and Tsung-Yi Lin. Magic3d: High-resolution text-to-3d content creation. In *Proceedings of the IEEE/CVF* Conference on Computer Vision and Pattern Recognition, pages 300–309, 2023. 2
- [19] Jonathan Lorraine, Kevin Xie, Xiaohui Zeng, Chen-Hsuan Lin, Towaki Takikawa, Nicholas Sharp, Tsung-Yi Lin, Ming-Yu Liu, Sanja Fidler, and James Lucas. Att3d: Amortized text-to-3d object synthesis. arXiv preprint arXiv:2306.07349, 2023. 2
- [20] Jianye Lu, Athinodoros S Georghiades, Andreas Glaser, Hongzhi Wu, Li-Yi Wei, Baining Guo, Julie Dorsey, and Holly Rushmeier. Context-aware textures. ACM Transactions on Graphics (TOG), 26(1):3–es, 2007.
- [21] Tom Mertens, Jan Kautz, Jiawen Chen, Philippe Bekaert, and Frédo Durand. Texture transfer using geometry correlation. *Rendering Techniques*, 273(10.2312):273–284, 2006.
- [22] Meshy. Meshy 3d ai generator. https://www.meshy.ai/, 2023. 6, 7
- [23] Gal Metzer, Elad Richardson, Or Patashnik, Raja Giryes, and Daniel Cohen-Or. Latent-nerf for shape-guided generation of 3d shapes and textures. In *Proceedings of the IEEE/CVF* Conference on Computer Vision and Pattern Recognition, pages 12663–12673, 2023.
- [24] Chong Mou, Xintao Wang, Liangbin Xie, Jian Zhang, Zhongang Qi, Ying Shan, and Xiaohu Qie. T2i-adapter: Learning adapters to dig out more controllable ability for text-to-image diffusion models. arXiv preprint arXiv:2302.08453, 2023. 3
- [25] Gimin Nam, Mariem Khlifi, Andrew Rodriguez, Alberto Tono, Linqi Zhou, and Paul Guerrero. 3d-ldm: Neural implicit 3d shape generation with latent diffusion models. arXiv preprint arXiv:2212.00842, 2022. 2
- [26] Alex Nichol, Heewoo Jun, Prafulla Dhariwal, Pamela Mishkin, and Mark Chen. Point-e: A system for generating 3d point clouds from complex prompts. ArXiv, abs/2212.08751, 2022. 2
- [27] Ben Poole, Ajay Jain, Jonathan T Barron, and Ben Mildenhall. Dreamfusion: Text-to-3d using 2d diffusion. *arXiv* preprint arXiv:2209.14988, 2022. 2
- [28] Emil Praun, Adam Finkelstein, and Hugues Hoppe. Lapped textures. In *Proceedings of the 27th annual conference on Computer graphics and interactive techniques*, pages 465–470, 2000.
- [29] Alec Radford, Jong Wook Kim, Chris Hallacy, Aditya Ramesh, Gabriel Goh, Sandhini Agarwal, Girish Sastry, Amanda Askell, Pamela Mishkin, Jack Clark, et al. Learning transferable visual models from natural language supervision. In *International conference on machine learning*, pages 8748–8763. PMLR, 2021. 2

- [30] Elad Richardson, Gal Metzer, Yuval Alaluf, Raja Giryes, and Daniel Cohen-Or. Texture: Text-guided texturing of 3d shapes. arXiv preprint arXiv:2302.01721, 2023. 1, 2, 5, 6, 7
- [31] Robin Rombach, Andreas Blattmann, Dominik Lorenz, Patrick Esser, and Björn Ommer. High-resolution image synthesis with latent diffusion models. In *Proceedings of* the IEEE/CVF conference on computer vision and pattern recognition, pages 10684–10695, 2022. 2, 3
- [32] Aditya Sanghi, Hang Chu, Joseph G. Lambourne, Ye Wang, Chin-Yi Cheng, Marco Fumero, and Kamal Rahimi Malekshan. Clip-forge: Towards zero-shot text-to-shape generation. In 2022 IEEE/CVF Conference on Computer Vision and Pattern Recognition (CVPR), pages 18582–18592, 2022. 2
- [33] Aditya Sanghi, Hang Chu, Joseph G Lambourne, Ye Wang, Chin-Yi Cheng, Marco Fumero, and Kamal Rahimi Malekshan. Clip-forge: Towards zero-shot text-to-shape generation. In Proceedings of the IEEE/CVF Conference on Computer Vision and Pattern Recognition, pages 18603–18613, 2022. 2
- [34] Edward J Smith and David Meger. Improved adversarial systems for 3d object generation and reconstruction. In *Conference on Robot Learning*, pages 87–96. PMLR, 2017. 2
- [35] Jascha Sohl-Dickstein, Eric Weiss, Niru Maheswaranathan, and Surya Ganguli. Deep unsupervised learning using nonequilibrium thermodynamics. In *International confer*ence on machine learning, pages 2256–2265. PMLR, 2015.
- [36] Christina Tsalicoglou, Fabian Manhardt, Alessio Tonioni, Michael Niemeyer, and Federico Tombari. Textmesh: Generation of realistic 3d meshes from text prompts. arXiv preprint arXiv:2304.12439, 2023. 5
- [37] Aaron Van Den Oord, Oriol Vinyals, et al. Neural discrete representation learning. Advances in neural information processing systems, 30, 2017.
- [38] Tien-Tsin Wong, Wai-Yin Ng, and Pheng-Ann Heng. A geometry dependent texture generation framework for simulating surface imperfections. In *Rendering Techniques' 97: Proceedings of the Eurographics Workshop in St. Etienne, France, June 16–18, 1997 8*, pages 139–150. Springer, 1997.
- [39] Chaohui Yu, Qiang Zhou, Jingliang Li, Zhe Zhang, Zhibin Wang, and Fan Wang. Points-to-3d: Bridging the gap between sparse points and shape-controllable text-to-3d generation, 2023.
- [40] Xiaohui Zeng, Arash Vahdat, Francis Williams, Zan Gojcic, Or Litany, Sanja Fidler, and Karsten Kreis. Lion: Latent point diffusion models for 3d shape generation. ArXiv, abs/2210.06978, 2022. 2
- [41] Lvmin Zhang, Anyi Rao, and Maneesh Agrawala. Adding conditional control to text-to-image diffusion models. In Proceedings of the IEEE/CVF International Conference on Computer Vision, pages 3836–3847, 2023. 3
- [42] Linqi Zhou, Yilun Du, and Jiajun Wu. 3d shape generation and completion through point-voxel diffusion. In *Proceedings of the IEEE/CVF International Conference on Computer Vision*, pages 5826–5835, 2021. 2